RESEARCH ARTICLE SUMMARY

MARTIAN GEOLOGY

Redox stratification of an ancient lake in Gale crater, Mars

J. A. Hurowitz,* J. P. Grotzinger, W. W. Fischer, S. M. McLennan, R. E. Milliken, N. Stein, A. R. Vasavada, D. F. Blake, E. Dehouck, J. L. Eigenbrode, A. G. Fairén, J. Frydenvang, R. Gellert, J. A. Grant, S. Gupta, K. E. Herkenhoff, D. W. Ming, E. B. Rampe, M. E. Schmidt, K. L. Siebach, K. Stack-Morgan, D. Y. Sumner, R. C. Wiens

INTRODUCTION: The primary goal of NASA's Curiosity rover mission is to explore and quantitatively assess a local region on Mars' surface as a potential habitat for past or present life. A necessary component of that assessment involves an investigation of the surface chemical conditions and paleoclimate of ancient Mars. Gale crater was selected as the landing site for Curiosity; it hosts a ~5-km-tall mountain of layered sedimentary rock. The rocks of Mount Sharp preserve a long-duration record of martian environmental conditions. Geological reconstructions from Curiosity rover data have revealed an ancient, habitable lake environment that was sustained for tens of thousands to tens of millions of years by rivers draining into the crater.

RATIONALE: We seek to constrain the chemical environment within the lake in Gale crater, as well as short- and long-term climate variations in and around Gale crater. We focus on fine-grained sedimentary rocks that carry information about sediment provenance, the environment of deposition, the conversion of sediment to rock during burial (i.e., lithification), and the chemical conditions of later modification (i.e., diagenesis). These were investigated during the first 1300 martian solar days (sols) of rover operations in Gale crater using bulk geochemical and mineralogical analysis techniques, combined with high-resolution color imagery at a variety of scales.

RESULTS: Two mudstone units have been recognized, both deposited in lakes: the Sheepbed member of the Yellowknife Bay formation, an older set of strata defining the base of the stratigraphic section; and the Murray formation, of relatively younger age and positioned higher in the stratigraphic section. The chemical index of alteration (CIA) paleoclimate proxy increases by up to ~10 to 20 CIA units (expressed in %) from the Sheepbed member to the Murray formation. On the basis of mineralogy, geochemistry, textural properties, and stratigraphic relationships, the Murray formation can be subdivided into two sedimentary associations, or facies: the hematite-phyllosilicate (HP) facies and the magnetite-silica (MS) facies. The HP facies is characterized by abundant Fe^{3+} oxides accompanied by phyllosilicates, as well as indications of Mn oxidation and trace metal concentration. These properties are consistent with deposition in an oxidizing environment. The MS facies is recognized by a near-complete absence of pure Fe^{3+} minerals, and high concentrations of silica accompanied by magnetite, consistent with deposition in an anoxic environment. Both facies were affected by a saline overprint after burial and lithification.

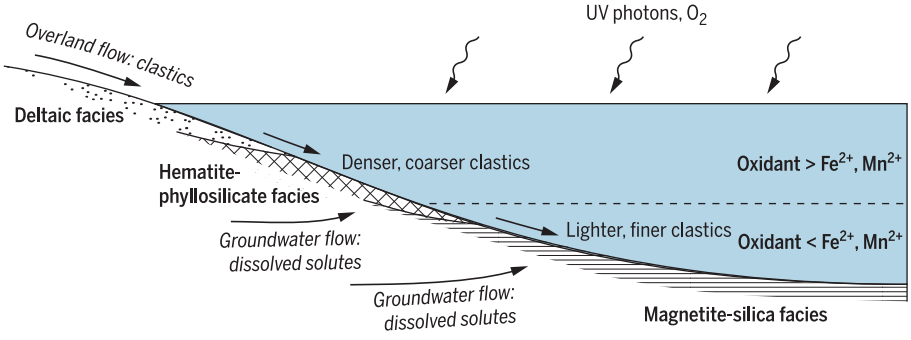

A hypothesized redox-stratified lake in Gale crater. Model of physical transport and geochemical processes occurring during deposition of the Murray formation. Fresh water and clastic materials are delivered by overland flow from fluvial systems; dissolved solutes enter the lake by groundwater seepage. Redox stratification results from differences in the mass balance of atmospheric oxidants and oxidizable cations, causing redox-sensitive mineral assemblages to vary as a function of lake water depth. Flow deceleration results in sediment fractionation into distinct sedimentological associations; coarser, denser clastic materials are deposited closer to shore (hematite-phyllosilicate facies), whereas finer, less dense clastics travel further into the lake (magnetite-silica facies). UV, ultraviolet.

CONCLUSION: The observed variations in CIA are consistent with modest short-term fluctuations in the ancient climate between cold, dry conditions and relatively warmer, wetter conditions. These changes occurred during the deposition of lake-bed mudstones in an environment that was conducive to the presence of a long-lived lake in Gale crater. We propose that the distinct properties of the two Murray facies were developed as a result of (i) fractionation of river-borne detritus into coarser, denser materials in shallow water close to shore and finer, lower density materials offshore in deeper water as a result of deceleration of river flow as it entered the lake; and (ii) redox stratification of the lake water body, caused by depth-dependent variations in the concentration of atmospheric oxidants and dissolved, groundwater-derived solutes, resulting in oxidizing conditions in shallow water and anoxia in deeper water. The addition of saline minerals during a later phase of brine migration through the section records longer-term changes in martian climate at Gale crater, perhaps driven by global atmospheric escape processes. The recognition of redox stratification in the lake in Gale crater adds new detail to our understanding of ancient martian aquatic environments. Previously reported detections of organic carbon compounds, nitrogen, phosphate minerals, and Fe and S minerals in a variety of redox states, combined with the evidence presented here for relatively stable climate conditions and gradients in fluid oxidation state, provide compelling evidence that all of the physical, chemical, and energetic conditions necessary to establish a habitable environment were present on Mars between ~3.8 billion and 3.1 billion years ago. ■

ON OUR WEBSITE

Read the full article at http://dx.doi.org/10.1126/science.aah6849

The list of author affiliations is available in the full article online.
*Corresponding author. Email: joel.hurowitz@stonybrook.edu
Cite this article as J. A. Hurowitz *et al.*, *Science* **356**, eaah6849 (2017). DOI: 10.1126/science.aah6849

RESEARCH ARTICLE

MARTIAN GEOLOGY

Redox stratification of an ancient lake in Gale crater, Mars

J. A. Hurowitz,[1]* J. P. Grotzinger,[2] W. W. Fischer,[2] S. M. McLennan,[1] R. E. Milliken,[3] N. Stein,[2] A. R. Vasavada,[4] D. F. Blake,[5] E. Dehouck,[6] J. L. Eigenbrode,[7] A. G. Fairén,[8,9] J. Frydenvang,[10,11] R. Gellert,[12] J. A. Grant,[13] S. Gupta,[14] K. E. Herkenhoff,[15] D. W. Ming,[16] E. B. Rampe,[17] M. E. Schmidt,[18] K. L. Siebach,[1,2] K. Stack-Morgan,[4] D. Y. Sumner,[19] R. C. Wiens[10]

In 2012, NASA's Curiosity rover landed on Mars to assess its potential as a habitat for past life and investigate the paleoclimate record preserved by sedimentary rocks inside the ~150-kilometer-diameter Gale impact crater. Geological reconstructions from Curiosity rover data have revealed an ancient, habitable lake environment fed by rivers draining into the crater. We synthesize geochemical and mineralogical data from lake-bed mudstones collected during the first 1300 martian solar days of rover operations in Gale. We present evidence for lake redox stratification, established by depth-dependent variations in atmospheric oxidant and dissolved-solute concentrations. Paleoclimate proxy data indicate that a transition from colder to warmer climate conditions is preserved in the stratigraphy. Finally, a late phase of geochemical modification by saline fluids is recognized.

Fine-grained sedimentary rocks deposited in lakes and oceans provide valuable proxy records of changes in Earth's dynamic surface environment. These rocks have been used to deduce the nature and extent of variations in global climate (*1*), the evolution of the composition of Earth's crust (*2*), and biologically driven changes in the redox state of Earth's atmosphere (*3*). Such rocks have the important property of containing detrital components that carry information about sediment provenance and weathering, and secondary minerals that carry information about the environment of deposition and lithification. In cases where postdepositional geochemical, mineralogical, and textural modification (diagenesis) has partly modified primary signals, it is often possible to decipher those changes to reconstruct past events (*4*, *5*). Given their importance to understanding Earth history, locales containing layered sedimentary rocks linked to depositional processes in rivers, lakes, and seas on Mars have also become a focal point for paleoenvironmental studies. Indeed, a primary motivation behind the selection of Gale crater as the landing site for the Mars Science Laboratory (MSL) Curiosity rover mission was the presence of a ~5-km-tall mountain of layered sedimentary rock, hypothesized to contain a long-duration record of secular changes in martian surface environments (*6*–*9*).

As it traversed toward Aeolis Mons (informally known as Mount Sharp), Curiosity has studied mudstones, sandstones, and conglomerates of the Bradbury group and younger mudstones and sandstones of the Murray formation (fm.) at the base of Mount Sharp (*10*, *11*). The lake-bed (lacustrine) mudstones of these two genetically related units form the focus of this study. These rocks are separated by ~60 m of stratigraphic thickness but are related by a common depositional setting (Fig. 1), allowing comparison of their chemical and mineralogical properties. This enables an evaluation of the geochemical and environmental history of the ancient lake system in Gale crater, placing constraints on its habitability and paleoclimate. The Murray fm. can be subdivided into two groups (facies): one that is recognized by abundant ferric iron–bearing minerals (e.g., hematite) accompanied by phyllosilicates and another that is recognized by high concentrations of silica minerals accompanied by magnetite. Mudstones of the Murray fm. show abrupt juxtaposition of these mineral facies, which requires either spatial or temporal variation in lake chemistry. Here we propose a model in which delivery of fine-grained detritus by rivers to a redox-stratified lake provides an explanation for the observed properties of the Murray fm. mudstones. The recognition of a stable redox-stratified water body adds important detail to our understanding of the potential for microbial chemoautotrophy within the ~3.8- to 3.1-billion-year-old Gale crater lake system.

Geological setting

Gale crater is situated in river-dissected terrain immediately south of the hemispherical topographic boundary between the cratered southern highlands and smooth northern lowland plains of Mars, known as the martian dichotomy boundary. Previous work shows that the crater formed ~3.8 billion to 3.6 billion years ago (Ga) (*9*, *12*). The central portion of the crater contains sedimentary deposits that form a large mound (Mount Sharp), possibly cored by a central peak (*9*, *11*–*13*). After formation, Gale crater was infilled with alluvial fan and lacustrine sediments that were deposited and exhumed before 3.3 to 3.1 Ga (*9*, *10*, *12*, *14*).

Curiosity landed on erosional remnants of a thick sequence (>75 m) of mostly fluvial-deltaic (i.e., river and near-shore) sandstones and conglomerates known as the Bradbury group, which contains a basal unit (Yellowknife Bay fm.) composed in part of lacustrine mudstones [Sheepbed member, Fig. 1, (*10*, *11*, *15*, *16*)]. To the south of Curiosity's landing site, the Bradbury group interfingers with, and is ultimately overlain by, lacustrine mudstones of the Murray fm., which is the lowest exposed unit of the Mount Sharp group. Both the Bradbury group and Murray fm. were buried to substantial depth (hundreds to thousands of meters) and then exhumed by eolian (wind) erosion (*10*). These rocks have been affected by burial diagenesis, including cementation, fracturing, and vein mineralization (*10*, *11*, *17*, *18*), in addition to early diagenetic textural modifications, including subaqueous shrinkage cracks, preserved gas bubbles, and nodules (*10*, *11*, *19*–*21*). A younger succession of eolian sandstones (Stimson fm.) overlies the Murray fm. as well as the Bradbury group and is separated from these underlying units by an erosional surface (i.e., an unconformity). Figure S1 shows a map of Curiosity's traverse and major geologic waypoints.

Lacustrine deposits of the Sheepbed member and the younger Murray fm. are predominantly composed of fine-grained rock (<64-μm grain size) displaying massive to laminated (millimeter- to centimeter-scale) bedding, characteristic of deposition under quiescent conditions (*10*, *11*). Intervals of the Murray fm. show features characteristic of episodic reworking of the lake floor and introduction of coarser sediments by prodeltaic or

[1]Department of Geosciences, Stony Brook University, Stony Brook, NY 11794-2100, USA. [2]Division of Geological and Planetary Sciences, California Institute of Technology, Pasadena, CA 91125, USA. [3]Department of Geological Sciences, Brown University, Providence, RI 02912, USA. [4]Jet Propulsion Laboratory, California Institute of Technology, Pasadena, CA 91109, USA. [5]Department of Space Sciences, NASA Ames Research Center, Moffett Field, CA 94035, USA. [6]Institut de Recherche en Astrophysique et Planétologie, University Paul Sabatier, 31028 Toulouse, France. [7]NASA Goddard Space Flight Center, Greenbelt, MD 20771, USA. [8]Centro de Astrobiología, Consejo Superior de Investigaciones Científicas–Instituto Nacional de Técnica Aeroespacial (CSIC-INTA), 28850 Madrid, Spain. [9]Department of Astronomy, Cornell University, Ithaca, NY 14853, USA. [10]Space Remote Sensing, Los Alamos National Laboratory, Los Alamos, NM 87544, USA. [11]University of Copenhagen, 1350 Copenhagen, Denmark. [12]Department of Physics, University of Guelph, Guelph, Ontario N1G 2W1, Canada. [13]Center for Earth and Planetary Studies, National Air and Space Museum, Smithsonian Institution, Washington, DC 20560, USA. [14]Department of Earth Science and Engineering, Imperial College London, London SW7 2AZ, UK. [15]U.S. Geological Survey, Flagstaff, AZ 86001, USA. [16]Astromaterials Research and Exploration Science Division, NASA Johnson Space Center, Houston, TX 77058, USA. [17]NASA Johnson Space Center, Houston, TX 77058, USA. [18]Department of Earth Sciences, Brock University, St. Catharines, Ontario L2S 3A1, Canada. [19]Department of Earth and Planetary Sciences, University of California–Davis, Davis, CA 95616, USA.
*Corresponding author. Email: joel.hurowitz@stonybrook.edu

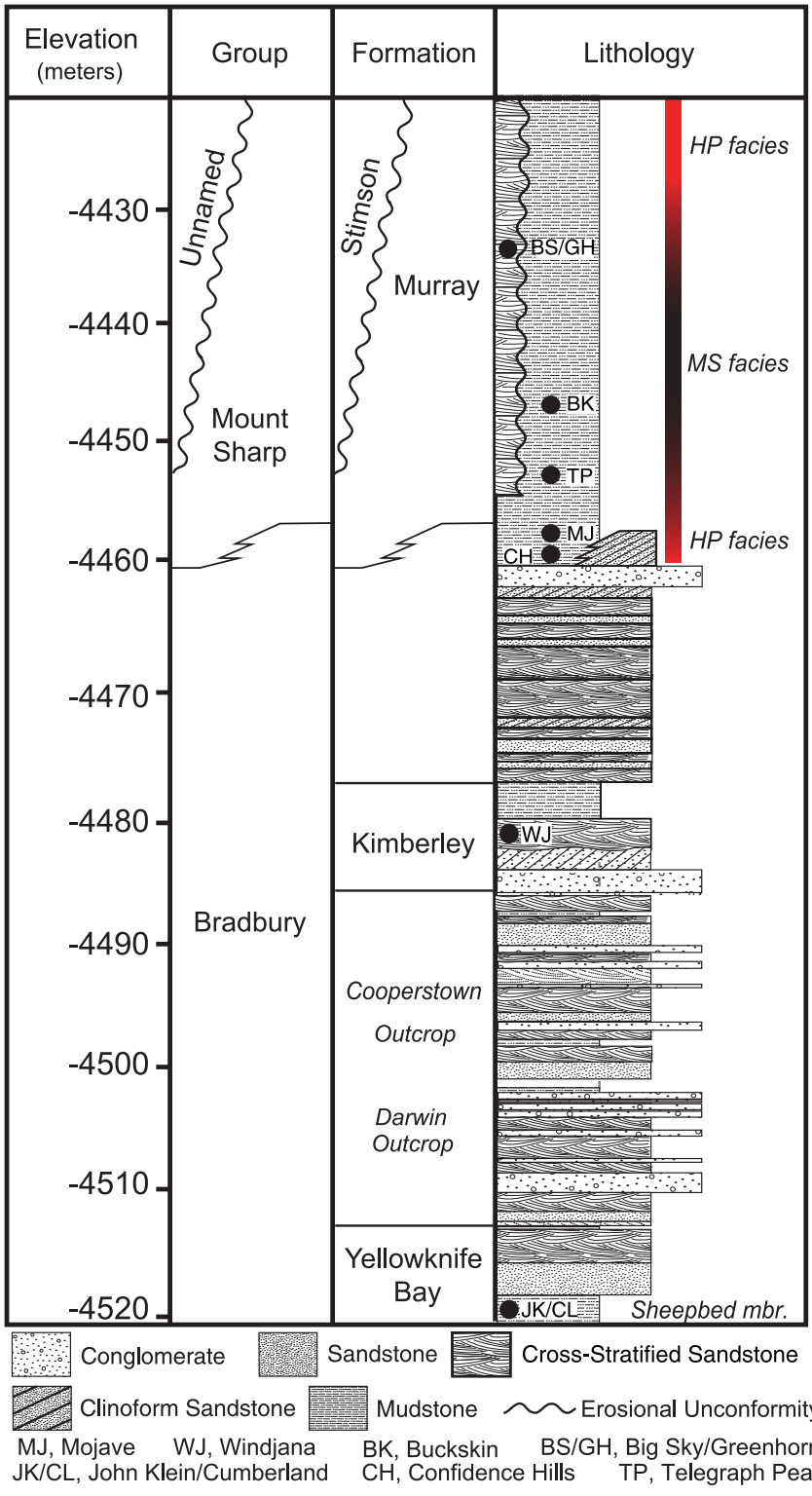

Fig. 1. Stratigraphic column for the sedimentary rocks of Gale crater through sol 1300. Adapted from (*10*). Drill samples are denoted by black circles; the sandstone drill targets Windjana (WJ), Big Sky (BS), and Greenhorn (GH) are not discussed in this paper. The contact between the Bradbury and Mount Sharp groups is interfingering in nature. Vertical repetition of the HP and MS facies occurs in the stratigraphy, as indicated by the black and red column on the right. The MS facies at Hidden Valley (Bonanza King sample, APXS only, fig. S1) is at about the same stratigraphic level as the MJ and CH samples from the HP facies at Pahrump Hills. Khomas and Sperrgebiet are located near the top of the section, in the cross-stratified sandstones of the Stimson fm. Elevations are referenced to the zero-elevation datum on Mars defined in (*86*).

fluvial transport, including scour-and-drape deposits, thin centimeter-scale coarser beds, and uncommon thin layers of cross-bedded sandstone (*10*). The lower Murray fm. shows no evidence for exposure of these sediments while they were wet (e.g., desiccation features), suggesting that this portion of the Gale lake system was perennial. Finally, for the lacustrine strata explored so far, characteristic signs of a glacial climate such as dropstones, diamictites, or ice-wedge fills have not been observed (*10*, *11*).

Through martian solar day (sol) 1300, x-ray diffraction (XRD) data (see methods) were obtained from six mudstone samples by the Chemistry and Mineralogy (CheMin) instrument (*22*) on board the Curiosity rover (Fig. 1). These samples include John Klein (JK), Cumberland (CL), Confidence Hills (CH), Mojave (MJ), Telegraph Peak (TP), and Buckskin (BK). The distinctive mineralogy of these mudstone samples enables their subdivision into three groupings: (i) the Sheepbed member (which includes JK and CL), (ii) the hematite-phyllosilicate (HP) facies of the Murray fm. (which includes CH and MJ), and (iii) the magnetite-silica (MS) facies of the Murray fm. (which includes TP and BK). On the basis of geochemical, stratigraphic, and sedimentological associations, these groupings can be extended to the full suite of mudstone samples that have been imaged and analyzed by the Curiosity instrument payload, but which have not been analyzed by XRD. The mineralogical and geochemical analysis techniques used in this paper are described in the methods, with data tabulated on table S1 and in data file S1.

Mudstone geochemistry

Gale crater mudstones have been influenced by a combination of (i) variation in source rock composition and degree of chemical weathering (i.e., provenance), (ii) physical sorting during transport and deposition, (iii) water-rock reaction during transport and deposition, (iv) redox and pH conditions within the lake, and (v) diagenetic processes. In Figs. 2 to 4, we describe geochemical relationships, derived from data collected with the Alpha Particle X-ray Spectrometer [APXS, methods, (*23*)], between and within mudstone suites to understand the influence of these different factors on proxy signals for paleoclimate and redox conditions.

The chemical index of alteration [CIA (%)] is plotted against SiO_2 [weight % (wt %)] in Fig. 2; CIA is calculated as the ratio $[Al_2O_3/(Al_2O_3 + Na_2O + CaO + K_2O)] \times 100$ in molar proportions, and together, CIA and SiO_2 provide information on sediment provenance, paleoweathering conditions, and mineral-addition processes. CIA and SiO_2 are positively correlated for the Sheepbed member and Murray HP facies, with the Sheepbed member displaying low CIA and SiO_2 and the HP facies displaying higher CIA and SiO_2. The MS facies occupies a distinctive position on the diagram, displaced from the HP facies toward intermediate CIA and high SiO_2. The CIA values calculated here are minima; they have not been corrected for phases that have the effect of lowering CIA when present (e.g., calcite, halite, gypsum). The effect of these phases on CIA can be accounted for, as

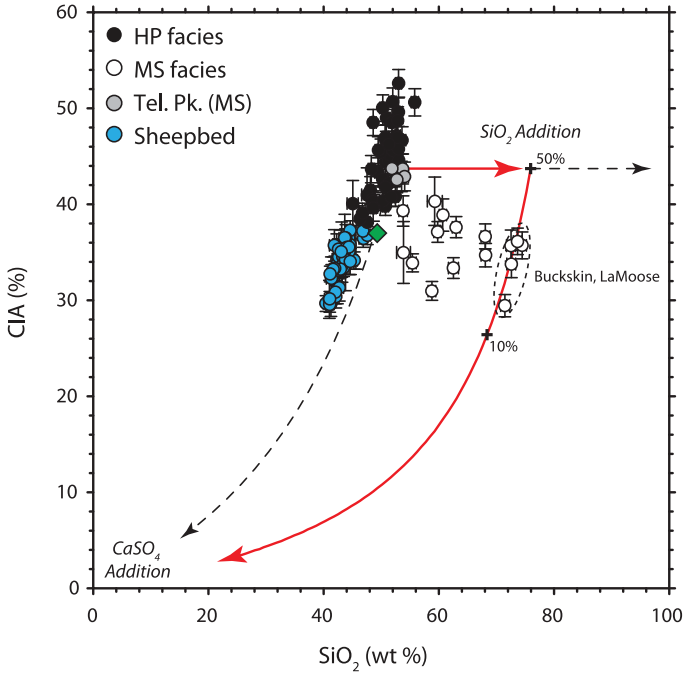

Fig. 2. Paleoweathering, provenance, and mineral addition in Gale crater mudstones. CIA (%) versus SiO_2 (wt %) showing climate-induced variations in mudstone geochemistry. Dashed arrowhead lines are mixing vectors between the MS facies sample named Telegraph Peak (Tel. Pk., gray circles), SiO_2, and $CaSO_4$. The red arrowhead line shows the vectors generated by a two-stage mixing model where Tel. Pk. and SiO_2 are mixed in 50:50 proportions, followed by the addition of $CaSO_4$ to the mixed composition. Average martian crust (*26*) is plotted with a green diamond.

discussed below and in the supplementary online text, including fig. S2.

CIA reflects the degree to which the sources of sedimentary rocks were chemically weathered before physical erosion and during transport to their depositional site (*24*, *25*). The Sheepbed member mudstones exhibit low CIA values that approximate the CIA of average martian crust, which is 37% (*26*). Accordingly, McLennan *et al.* (*27*) argued that these low CIA values indicate that the sources of these mudstones experienced little to no chemical weathering, consistent with sediment generation and transport under cold and/or arid conditions. In contrast, the HP facies exhibits higher CIA values and SiO_2 concentrations relative to those of the Sheepbed member and average martian crust. A reasonable first-order interpretation is that these elevated CIA values indicate a shift in climate toward conditions that allowed chemical weathering processes to modify the sources of the HP facies and increase their CIA values.

The change in CIA between average Sheepbed member mudstone (34 ± 2%) and HP facies mudstone (45 ± 4%) is 11%, and when the CIA values of the lowest SO_3 mudstone analyses are compared, the difference is 16.1% (supplementary text, fig. S2). These differences might reflect a change from cold to temperate climate conditions in the sediment source regions (*1*, *24*). As stated above, the low CIA values of the Sheepbed member are readily interpreted in terms of a cold and/or arid climate (*27*), implying that climate conditions were comparatively warmer or wetter during deposition of the Murray fm. However, our understanding of the behavior of CIA in basaltic sedimentary systems is more limited in comparison to sediments generated from the felsic sources that dominate Earth's upper continental crust. Terrestrial sedimentary rocks are typically generated from sources that have a CIA value of ~45 to 50% and evolve to higher values (*28*). Therefore, we conservatively interpret the differences in CIA shown in Fig. 2 in terms of climate variation from colder and drier to warmer and wetter but cannot infer a specific climate condition in the sediment source regions of the Gale mudstones.

The observed correlation between CIA and SiO_2 is also likely related to variations in the extent of chemical weathering in the sediment source regions. Weathering reactions are expected to liberate aqueous silica to solution (*29*, *30*), thereby increasing the silica concentration of fluids transporting detrital sediment toward Gale crater. Ultimately, this silica would have precipitated in the lacustrine environment during and after deposition of detrital materials. Another possible explanation for the observed correlation is that the igneous sources of HP facies detritus were more evolved (felsic) than those of the Sheepbed member. In this case, the SiO_2 content and CIA of the clastic material in the HP facies would naturally be elevated relative to the less evolved (mafic) clastic material in the Sheepbed member. Indeed, a comparison of the crystalline mineralogy of the Sheepbed member and the Murray fm. indicates that the ratio feldspars/(pyroxenes + olivine) is higher for the Murray fm. than the Sheepbed member [table S1 and (*31*)]. In addition, some fluvial sandstones and conglomerates observed along Curiosity's traverse exhibit felsic characteristics (*32*–*35*). However, felsic igneous rocks with CIA values of ~50% (e.g., rhyolites and granites) typically have SiO_2 concentrations of 70 to 75 wt % (*36*). The SiO_2 content of the HP facies (51 ± 2 wt %), although elevated compared to the Sheepbed member (43 ± 2 wt %), is not high enough for the differences in CIA between the Sheepbed member and the HP facies to be explained entirely by variations in the proportions of mafic and felsic sources. Accordingly, we interpret the observed correlation between CIA and SiO_2 to result predominantly from chemical weathering processes in the sediment source regions.

Even higher SiO_2 concentrations are observed in the Murray MS facies, consistent with high abundances of crystalline and amorphous silica-rich phases observed in XRD data [see below and (*31*)]. Low to moderate CIA values are also observed. APXS analyses of samples from the target named Telegraph Peak have among the lowest SiO_2 (52 to 54 wt %) and highest CIA (43%) values of the MS facies. This sample therefore makes a reasonable starting composition from which to model the effects of mineral addition on whole-rock chemistry and better understand the variations in APXS data from the MS facies. The addition of pure SiO_2 results in a horizontal vector in Fig. 2 that does not match the scattered negative relationship between CIA and SiO_2. Fracture- and void-filling $CaSO_4$ phases are a ubiquitous feature of the sedimentary units in Gale crater that appear to have been emplaced during postlithification diagenesis (*11*, *17*). A modeled mixture between Telegraph Peak and pure $CaSO_4$ also does not match the chemical variation displayed by the MS facies (but does provide another mechanism by which positive correlations between CIA and SiO_2 could be generated). Although neither the addition of SiO_2 nor $CaSO_4$ can explain the position of the MS facies in Fig. 2 on their own, we do find that a two-stage addition model, where SiO_2 is first added to Telegraph Peak followed by $CaSO_4$ addition, provides a reasonable first-order description of the observed bulk chemical variability of the MS facies. The highest silica analyses in the MS facies (Buckskin, LaMoose) require a 50:50 mixture of Telegraph Peak and SiO_2, followed by the addition of ~2 to 7% $CaSO_4$, to match their positions. Samples with lower SiO_2 contents and higher CIA values than Buckskin require correspondingly lower amounts of silica and $CaSO_4$ addition. An implication of this model is that the original CIA values of the MS facies were higher than observed but have been depressed by the presence of Ca sulfate in the APXS field of view (also see supplementary text and fig. S2). The MS facies also exhibits elevated TiO_2 and P_2O_5 concentration (fig. S3, A and B); possible causes for these elevated concentrations, and potential mineralogical hosts of TiO_2, are discussed in the supplementary text.

Figure 3A plots Zn [parts per million (ppm)] against MnO (wt %), and Fig. 3B plots Ni (ppm) against MnO (wt %). This suite of elements illustrates processes of oxidation and associated trace-metal enrichment, as well as trends developed as a result of dilution processes, during deposition in the lake and continuing during diagenesis. MnO and Zn are positively correlated in the Murray HP facies [regression slope 7500 ± 825, $r^2 = 0.69$]. The Murray MS facies samples also exhibit correlated behavior but are excluded from the regression

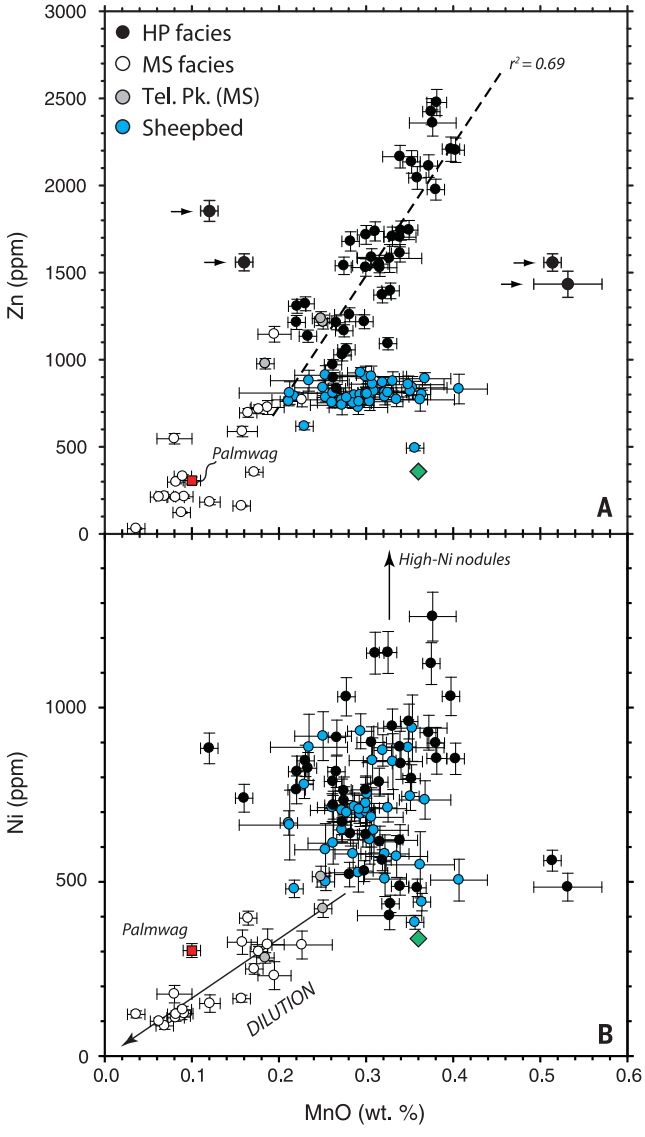

Fig. 3. Mn oxidation, metal scavenging, and dilution in the Murray fm. (**A**) Zn (ppm) versus MnO (wt %) showing a linear regression for the HP facies that results from Mn oxidation and scavenging of aqueous Zn by Mn oxides (the outlier samples Ricardo_Raster_1, Ricardo_DRT_1, Kleinberg, and Schwarzrand are excluded from the regression and labeled with arrowhead lines). (**B**) Ni (ppm) versus MnO (wt %) demonstrating dilution of MnO and trace metals in the MS facies by the addition of SiO_2 and $CaSO_4$, with data trending toward the origin. Green diamond is average Martian crust. The red square is target "Palmwag."

for reasons discussed below. The Sheepbed member exhibits no obvious trend, with MnO content ranging between ~0.2 and 0.4 wt % and Zn concentrations roughly constant for all samples. In Fig. 3B, neither the Murray HP facies nor the Sheepbed member samples exhibit correlated behavior between Ni and MnO. Both suites of samples are generally enriched in Ni relative to average martian crust, but in this case, the HP facies is indistinguishable from the Sheepbed member. The only exception is a suite of analyses on diagenetic concretions from the base of the HP facies at Pahrump Hills (figs. S1 and S4A), which exhibit high Ni concentrations, ranging from 1934 to 4169 ppm, and MnO concentrations ranging from 0.21 to 0.35 wt %. The MS facies is displaced from the HP facies and the Sheepbed member toward the origin.

For the HP facies, the observed correlation between MnO and Zn can be explained by Mn oxidation and precipitation coupled to scavenging and concentration of Zn from the water column or pore waters during deposition. Mn oxides are highly effective trace metal scavengers that are capable of adsorbing dissolved metal cations to their charged surfaces [e.g., (*37*)]. This process was invoked to explain the high MnO and Zn concentrations observed in fracture-filling materials between sols 600 and 630 at the Kimberley outcrop [fig. S1, (*38*)]. A second process that may have generated the apparent correlation between MnO and Zn is dilution by chemical and/or mineralogical components that are MnO and Zn free; this would drive samples toward the origin shown in Fig. 3A. In particular, MnO and Zn in the MS facies samples may have been diluted by the addition of silica and Ca sulfate discussed above (Fig. 2). An example of dilution is provided by an analysis of a Ca sulfate–vein target named Palmwag (fig. S4B), which exhibits the lowest MnO and Zn concentrations of any Murray fm. analysis. Analyses of the MS facies sample Telegraph Peak show that it has among the highest MnO and Zn and lowest SiO_2 and SO_3 concentrations in the MS facies, whereas the remaining MS facies samples, which generally exhibit higher SiO_2 and SO_3, are correspondingly lower in MnO and Zn. These lines of evidence support the hypothesis that dilution played a role in defining the systematics displayed by the MS facies shown in Fig. 3A.

The process of dilution in the MS facies is also illustrated in Fig. 3B. Although the HP facies and Sheepbed member are both enriched in Ni relative to the average crust of Mars, neither displays correlated behavior between Ni and Mn, and the two suites are indistinguishable from one another in terms of Ni and Mn content. The MS facies, in contrast, is correlated in Mn-Ni space, but in this case, the trend is toward the origin, consistent with a process of dilution by a component that has little to no Mn, Ni, or Zn in it, most likely silica and Ca sulfate. The lack of correlation between MnO and Ni for the HP facies indicates that the process of Mn oxidation and Zn scavenging, hypothesized above, did not have an effect on Ni, despite the fact that both of these metals are expected to be enriched by adsorption on Mn oxides (*37*). We suggest that the Mn, Zn, and Ni relationships displayed by the HP facies indicate that the primary lake waters from which Mn oxidized and precipitated were relatively Zn rich and Ni poor.

Figure 4 shows wt % MgO versus wt % SO_3. These two oxides illustrate the influence of saline fluids on bulk composition. Accordingly, Fig. 4 includes an additional set of samples from the Murray HP facies that are characterized by the presence of sulfate-rich diagenetic concretions, cross-cutting Ca sulfate veins, and/or total SO_3 concentrations >9.5 wt % (data file S1). The Sheepbed member exhibits a flat to slightly negative trend in Fig. 4. In contrast, the HP facies samples exhibit a scattered positive linear correlation between MgO and SO_3 (slope = 0.33 ± 0.05, r^2 = 0.49) when diagenetic and high SO_3 samples are included. As a group, the Murray MS facies does not appear to exhibit correlated behavior between MgO and SO_3. However, when we exclude analyses of the drill cuttings and tailings piles from the sample Buckskin, which exhibit low MgO (0.5 to 1.9 wt %), the remaining MS facies samples exhibit a weak positive linear correlation (slope = 0.27 ± 0.11, r^2 = 0.31), consistent with that exhibited by the HP facies. A suite of analyses of diagenetic concretions in the Stimson fm. (targets Sperrgebiet and Khomas, fig. S4C) provide an additional example of MgO-SO_3 correlation. These targets are offset to high total MgO but also exhibit a positive linear correlation between MgO and SO_3 with a regression slope (0.31 ± 0.01, r^2 = 0.99) that is identical (within error) to that exhibited by the Murray fm. samples. The positive linear correlations observed in Fig. 4 cannot be explained by rock-surface contamination by Gale crater soils, which have an average composition of 8.6 ± 0.9 wt % MgO and 4.6 ± 1.2 wt % SO_3 (average ± 1 standard deviation of 10 soil analyses collected between sols 0 and 1184, data file S1), or by atmospheric dust measured at Gale crater, which has identical MgO content to Gale crater soils and SO_3 content between 8.0 and 8.3 wt % (*39*).

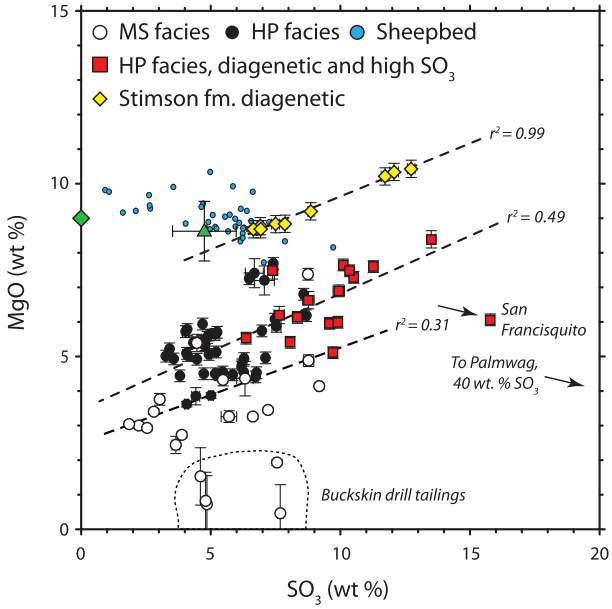

Fig. 4. Magnesium and calcium sulfates in the Murray fm. MgO (wt %) versus SO_3 (wt %), including HP facies analyses from diagenetic and high SO_3 samples (red squares) and diagenetic targets in the Stimson fm. (Khomas and Sperrgebiet, yellow diamonds). HP facies and Stimson fm. targets exhibit linear correlations with slopes of 0.33 ± 0.05 and 0.31 ± 0.01, respectively. When low-MgO analyses of drill tailings from the target Buckskin are excluded, the MS facies also exhibits a positive correlation with slope 0.27 ± 0.11. The slopes of the regression lines are lower than 0.5, as expected for Mg sulfate, and consistent with a mixture of Mg- and Ca-sulfate. Average Gale soil is shown with a green triangle, the green diamond is average Martian crust, and Sheepbed member is plotted here with small blue circles for clarity.

The positive linear regressions displayed between MgO and SO_3 in Fig. 4 indicate that Mg sulfate salts play an important role in the HP facies and possibly in the MS facies as well. In some cases, these salt enrichments occur as large, centimeter-scale concretionary or dendritic features [(*10*, *40*), fig. S4A], but in many cases, they lack a clear textural expression, suggesting the salts may be a component of the fine-grained mudstone matrix or cement. The CheMin instrument has not detected crystalline Mg sulfate phases, suggesting that this component is present in an amorphous or nanocrystalline state. The goodness-of-fit (r^2) of linear correlations between these two oxides scales inversely with the SiO_2 concentration of the group of samples through which the linear regression is drawn. Silica ranges from 39 to 43 wt % for the Khomas and Sperggebiet nodules from the Stimson fm. (r^2 = 0.99), from 43 to 54 wt % for the HP facies samples (r^2 = 0.47), and from 54 to 73 wt % for the MS facies samples (r^2 = 0.31). Thus, it may be that as the Mg sulfate component in these rocks is diluted by increasingly higher SiO_2 concentrations, our ability to effectively discern Mg sulfate in a bulk chemical analysis decreases. Finally, the slopes of the linear regressions for the MS facies (0.27 ± 0.11), HP facies (0.33 ± 0.05), and Stimson fm. (0.31 ± 0.01) targets are shallower than that of Mg sulfate minerals, which are characterized by an $MgO:SO_3$ weight ratio of 0.5. The shallow slopes can be explained by the incorporation of $CaSO_4$, which would have the effect of depressing the regression toward high SO_3, as shown in Fig. 4. As evidence, two samples from the HP facies (San Francisquito and Palmwag), which intentionally targeted cross-cutting Ca sulfate veins, trend away from the HP samples toward lower MgO and higher SO_3 concentrations.

Mudstone mineralogy

In Fig. 5, we describe mineralogical relationships derived from data collected using the CheMin instrument to further constrain the nature of sediment source regions and chemical conditions (e.g., pH, redox state) within the lake. We tabulated mineral abundances (Fig. 5A, table S1) in four groups: salts, amorphous, clastic, and probable secondary and redox-sensitive mineral phases. "Salts," detected at low concentrations (<5 wt %) in the Sheepbed member and in the MS facies sample Buckskin, primarily represent detections of the Ca sulfate minerals anhydrite and bassanite. These fracture-filling materials were intentionally avoided during drill-sample acquisitions, so their low abundances are expected. "Amorphous" is an x-ray amorphous component with variable chemical composition (*18*, *31*, *41*), present at 27 to 54 wt % abundance. "Clastic," which varies between ~40 and 50 wt % abundance, includes the following detrital crystalline minerals of probable igneous origin: feldspars, pyroxenes, olivine, quartz, cristobalite, tridymite, ilmenite, and apatite.

The "probable secondary and redox-sensitive mineral phases" group (Fig. 5B, table S1) makes up the remaining ~10 to 25 wt % of phases detected by CheMin. This group includes opal–cristobalite-tridymite (CT), phyllosilicates, the ferric sulfate mineral jarosite, Fe sulfides (mainly pyrrhottite of probable detrital origin), ferric iron oxides (hematite in the Murray fm., akaganeite and lesser hematite in the Sheepbed member), and the mixed-valence iron oxide magnetite. In the Sheepbed member, this group is dominated by phyllosilicate [specifically Fe-Mg smectite, (*18*, *42*)], with lesser magnetite, ferric oxides, and Fe sulfides, in decreasing order of abundance. The HP facies samples Confidence Hills and Mojave contain phyllosilicate, most likely a 2:1-layer phyllosilicate such as a collapsed smectite or illite (*41*), at lower abundance than in the Sheepbed member. The Confidence Hills sample also contains hematite, magnetite, and jarosite, in decreasing order of abundance; these four phases are present in subequal abundances in Mojave. The MS facies is largely composed of opal-CT and magnetite, with minor hematite and jarosite in the Telegraph Peak sample. No phyllosilicates are observed in the MS facies.

The grouping of mineral and amorphous components illustrates processes that influenced the mineralogical composition of mudstones in Gale crater (Fig. 5A). A large proportion of all mudstones is made up of crystalline minerals of likely igneous origin that were transported by fluvial systems as clastic sediment. If we allow for the possibility that the amorphous component is also detrital in origin, noting that it has been interpreted as a mixture of volcanic glasses and secondary phases plausibly formed by chemical alteration of that glass (*18*, *31*, *41*, *43*), and combine the amorphous and crystalline group abundances, then the total ranges from ~70 to 90 wt %. This large fraction of detrital igneous components stands in contrast to measurements of terrestrial Phanerozoic mudrocks, which contain on average 35 to 40 wt % detrital igneous minerals (predominantly quartz and feldspar), with the balance made up mostly of recycled sedimentary rock (*44*, *45*). A lack of active plate tectonics on Mars would contribute to limited or absent sediment recycling at Gale crater (*46*). Therefore, we suggest that the high abundance of detrital primary igneous minerals and amorphous phases in the mudstones of Gale crater reflect that they are first-cycle sediments that directly sample their igneous provenance(s).

Variations displayed by the "probable secondary and redox-sensitive mineral phases" group (Fig. 5B) indicate considerable differences in fluid chemical conditions during deposition of the mudstone sample suites. Sheepbed mineralogy is thought to reflect smectite and magnetite crystallization during sediment deposition and burial (i.e., during authigenesis), resulting from water-rock reactions with detrital clastic phases under moderate to alkaline pH, and anoxic to poorly oxidizing conditions (*18*, *27*, *47*). The presence of detrital pyrrhotite (plus minor pyrite) supports these conclusions regarding oxidation state, as do experiments indicating that authigenic magnetite can readily form from the spontaneous disproportionation of ferrous hydroxide precipitated under anoxic, alkaline conditions (*48*, *49*). The generation of akaganeite might reflect redox disequilibrium in the primary fluids from which magnetite and smectite precipitated, a common feature in terrestrial basaltic aquifers (*50*), or might record later diagenetic modification by more oxidizing fluids.

Further constraints on Gale lake chemistry are provided by the Murray fm., which shows internal stratigraphic variations in the secondary and redox-sensitive mineral assemblage. The HP facies contains smectitic or illitic clay, and the elevated CIA values observed for the HP facies (Fig. 2) indicate that chemical-weathering reactions were

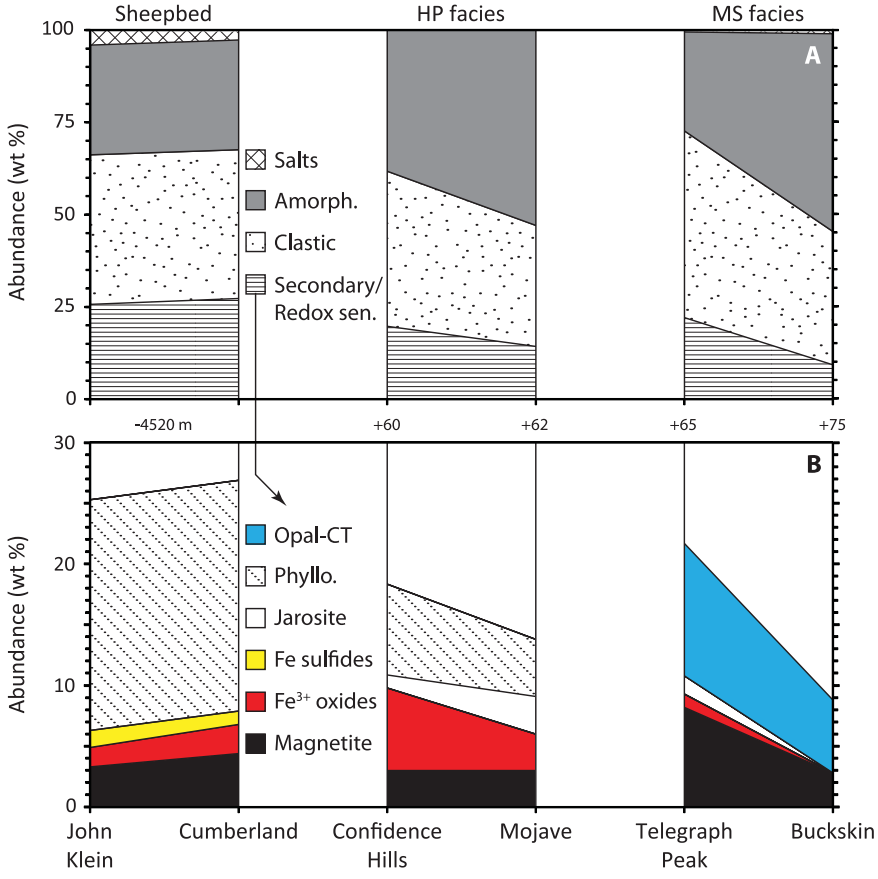

Fig. 5. Mineralogical composition of mudstones in Gale crater. (**A**) Total abundance (wt %) of crystalline salts, amorphous material, crystalline clastic phases of igneous origin, and the combination of secondary phases and redox-sensitive minerals. (**B**) Detail of secondary and redox-sensitive–mineral abundances. Differences in the nature and abundance of these phases imply considerable variability in lake-water chemistry. Sheepbed member samples were collected at −4520-m elevation; the heights above that datum for Murray fm. samples are indicated by values between the bar charts.

more active in the source regions of the HP facies. Accordingly, some or all of the phyllosilicate in the HP facies may be detrital, reflecting the mineralogy of the sediment source regions [e.g., (*51*)]. Phyllosilicate in the HP facies could also reflect precipitation from neutral to alkaline lake and/or pore waters during authigenesis, similar to the Sheepbed member. The Murray HP facies is characterized by a more oxidized mineral assemblage than the Sheepbed member, with ferric iron bearing secondary minerals present in greater abundance than mixed-valence iron–bearing species. If we assume that the magnetite in the HP facies is authigenic, similar to what was inferred for the Sheepbed member, then redox disequilibrium or evolving redox conditions during mineral authigenesis are implied. The presence of jarosite in the HP facies requires the activity of acidic fluids, between pH ≈ 2 and 4, which can be readily achieved by the oxidation of sulfide minerals (*52*). Only ~1.7 wt % detrital pyrrhotite, which is only ~0.5 wt % more than the quantity of detrital pyrrhotite observed in the Sheepbed member, would be required to generate the maximum observed jarosite in the HP facies (3.1 wt % in the Mojave_2 sample). Although CheMin analysis of the HP facies does not indicate the presence of sulfide minerals, the rapid rate of sulfide reaction under oxidizing conditions (*53*) could readily explain their absence. We suggest that the low-pH conditions implied by small amounts of jarosite do not reflect broader, basin-scale pH conditions but rather were localized to the immediate vicinity of oxidizing fluids in contact with sulfide grains, a phenomenon observed in numerous terrestrial examples [e.g., (*54*)].

In the MS facies, the total abundance of secondary and redox-sensitive phases varies by more than a factor of 2, and the assemblage is composed almost entirely of opal-CT and magnetite. Possible explanations for the appearance of opaline silica and disappearance of phyllosilicates in the MS facies include the following: (i) Detrital tridymite and cristobalite, present in high abundance in the MS facies, are unstable in surface waters and are expected to decompose to amorphous silica via mineral-water reaction (*55*, *56*). The high abundance of these thermodynamically unstable igneous silica minerals may have favored the production of high-silica pore fluids from which opaline silica precipitated. (ii) Another possibility, suggested by Morris *et al.* (*31*), is that opaline silica in the MS facies is detrital in origin. Finally, the MS facies contains extremely low abundances of pure ferric iron–bearing minerals; the near absence of such phases is consistent with anoxic to poorly oxidizing water conditions.

Chemical evolution of the Gale lake system

A simple process model of the lake-basin physiography, sediment transport, and chemistry can be used to explain the observations described above for Murray mudstones (Fig. 6). Fluvial-runoff draining the rim of Gale crater transported clastic detritus (*15*, *16*) and fresh water (*18*, *27*) to the lake. Gale crater is the lowest point for a thousand kilometers in any direction (*10*), which would have made it a locus for groundwater flow derived from the northward-dipping proximal southern highlands. Therefore, in addition to the freshwater and clastic materials delivered by surface fluvial systems, it is likely that groundwater seepage into the lake bed would have provided an additional source of solutes, such as dissolved SiO_2 (aq), Fe^{2+}, Mn^{2+}, Zn^{2+}, and other ions derived from reactions between water and rock along the regional groundwater flow path. These ions represent the raw materials from which some of the nondetrital secondary minerals could have formed.

Sediment transport from the crater rim and central peak resulted in hydrodynamic sorting that created wedges of fluvial, deltaic, and lacustrine sediments that thinned and fined toward the lake, located in the moat between the crater rim and central peak (*10*). As fluvial waters entered the proximal part of the lake, flow expansion and deceleration deposited thickly laminated sediment and, further offshore, thinly laminated facies representing the tail ends of dispersed plumes (fig. S4, D to F). The decelerating sediment plume would also fractionate clastic detritus so that distal parts would be enriched in lower density materials relative to their near-shore equivalents. Measurements of lamination thicknesses in the Murray fm. show that Si concentration increases and Fe concentration generally decreases with decreasing lamination thickness (fig. S5, A and B). Accordingly, the thicker lamination with more mafic mineralogy (table S1) and silica-poor composition of the Murray HP facies is consistent with its deposition in the proximal, shallower portion of the lake. Conversely, the thinner lamination, siliceous mineralogy (table S1), and more silica-rich composition of the Murray MS facies is consistent with its deposition in a more distal, deeper portion of the lake.

The correlation between the physical and mineralogic attributes of the two Murray lacustrine facies, and their reconstructed paleogeography and bathymetry, allows further development of the lake model. In particular, we can explain why the redox-sensitive mineralogy of the shallow-water HP facies is distinctly different from the deeper-water MS facies. We propose that redox stratification of the lake water body provides a reasonable hypothesis for the differences between these two

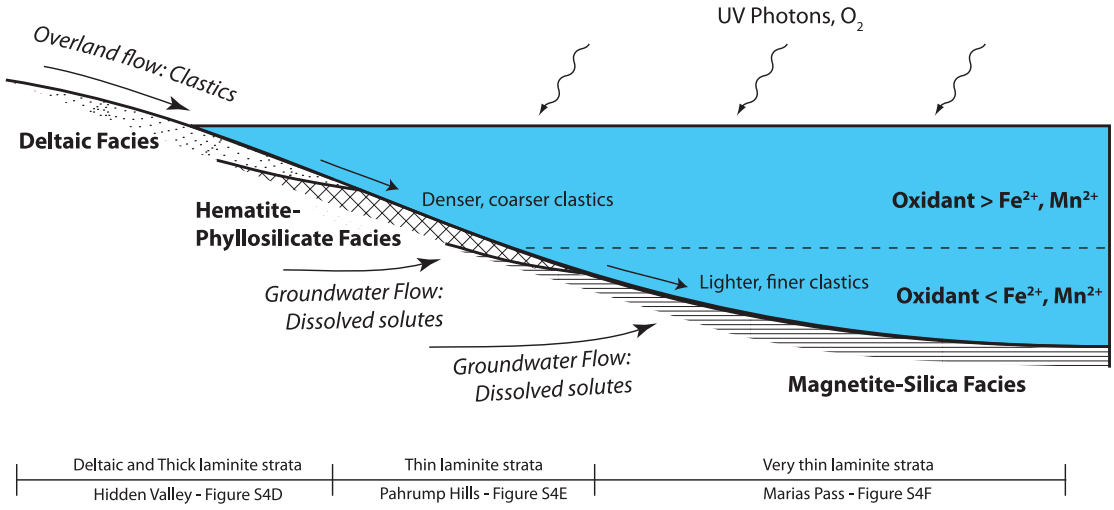

Fig. 6. A hypothesized redox-stratified lake in Gale crater. Model of physical transport and geochemical processes occurring during deposition of the Murray fm. Fresh water and clastic materials are delivered by overland flow from fluvial systems; additional dissolved solutes enter the lake by groundwater seepage. Deceleration of the incoming river flow produces characteristic changes in bedforms and sedimentary textures. These are described at the bottom of the diagram with examples from Curiosity's traverse where such bedforms have been observed (fig. S4, D to F). Flow deceleration also results in sediment fractionation; coarser, denser clastic materials are deposited closer to shore, whereas finer, less dense clastics travel further into the lake (also see fig. S5, A and B). Redox stratification results from differences in the mass balance of atmospheric oxidants (UV photons, O_2) and oxidizable cations (Fe^{2+}, Mn^{2+}), causing redox-sensitive mineral assemblages to vary as a function of lake water depth.

mineralogic facies and describes an abiotic mechanism of redox stratification for this martian lake. The model depends on the depth of penetration of ultraviolet (UV) light and low levels of photochemically generated atmospheric O_2 into the water column to establish a depth-dependent boundary between oxidized and anoxic zones (Fig. 6). Estimation of the depth of the redox transition between oxidized and anoxic waters has a nonunique solution that depends on the concentration of dissolved Fe^{2+} (and Mn^{2+}), the UV-photon flux reaching the lake surface, the effect of water-column turbidity on UV-light attenuation, the partial pressure of ancient atmospheric O_2, the kinetics of gas exchange at the lake-atmosphere interface, and mixing with depth. Measurements of deltaic clinoform thicknesses indicate that the water depths of the most proximal facies were on the order of 1 to 4 m (*10*), but the maximum depths of the lake are unconstrained by Curiosity data.

In the schematic model displayed in Fig. 6, dissolved, oxidizable cations (Fe^{2+} and Mn^{2+}) are delivered to the lake primarily by groundwater seepage through lake-floor sediments, whereas oxidants penetrate downward from the lake's upper surface. In the shallow portion of the lake, oxidant concentration exceeds that of dissolved Fe^{2+} and Mn^{2+}, so these cations are largely oxidized and precipitate as oxidized minerals, e.g., hematite and Mn oxide. The generation of Mn oxide in the shallow, oxidized portion of the lake results in the scavenging and enrichment of Zn^{2+} described previously. The relatively low average FeO/MnO ratio of the HP facies (56 ± 20) compared to the MS facies (73 ± 19) supports the hypothesis that Mn bypassed the anoxic portion of the lake but was retained in the oxidized part. The presence of low-pH waters, conducive to the small amount of jarosite precipitation that is observed in the HP facies, can be accommodated within the framework of shallow-water oxidative processes. Detrital sulfide minerals would have been oxidized after nearshore deposition, producing locally acidic porewater fluids. Meanwhile, the lake water body was likely characterized by neutral to alkaline pH values conducive to preservation and/or precipitation of the phyllosilicates observed in the HP facies. Below the depth of penetration of atmospheric oxidants, in the deeper portion of the lake, the waters remain largely anoxic, and under these conditions, the precipitation of authigenic magnetite is favored over more oxidized secondary iron minerals. Ferric iron minerals that settled out into the deeper, anoxic part of the lake could also have undergone reduction by dissolved inorganic ferrous-iron complexes [e.g., (*57*)] or by H_2 gas, which is a by-product of authigenic magnetite precipitation (*49*), with the net result being a paucity of pure ferric minerals in this part of the lake.

Neoproterozoic iron formations, which make a brief appearance at ~710 million years ago in the terrestrial rock record (*58*), may provide a useful process analog to the lacustrine mudstones of Gale crater. Unlike their ancient Archean and Paleoproterozoic counterparts, it appears that these iron formations have not interacted strongly with organic matter (*59*). The occurrence of these Fe-rich deposits at a time in Earth's history that postdates the rise of atmospheric oxygen [e.g., (*3*)] implies that Neoproterozoic seawater was, at times, capable of transporting and concentrating ferrous iron in solution and that the process responsible for oxidizing iron in seawater may have been a simple redox titration involving atmospheric oxidants (*60*, *61*), similar in some respects to what we propose for the shallow portions of the lake represented by the Murray HP facies.

A final component to consider in the context of the stratified lake model is the enrichment of the Murray fm. in Mg and Ca sulfate. Sulfate salts, particularly Mg sulfates, are extremely soluble and precipitate from highly concentrated, saline fluids [e.g., (*62*)]. Such fluids could readily form via evaporative concentration of lake waters, a scenario that bears some similarity to terrestrial acid-saline lake analogs (*63*–*65*). However, in the HP facies, where saline solutions seem to have most affected bulk sediment composition, physical sedimentary structures diagnostic of subaerial exposure and evaporation—such as desiccation cracks, prism cracks, curl-up laminae, fenestrae, intraclasts and rip-up chips, and centimeter-scale wave oscillation ripples (*66*–*70*)—are absent (*10*). Most notably, primary bedded evaporites and early diagenetic evaporite minerals with displacive growth geometry are absent. In the Murray HP facies, the highest concentrations of MgO and SO_3 are most closely associated with burial diagenetic features, such as nodules and dendrites (Fig. 3 and fig. S4A). These observations indicate that instead of a primary evaporitic origin, the saline component was added to the Murray fm. during or after burial and lithification. Diagenetic and high-SO_3 targets in the HP facies also display correlated behavior in MnO-Zn space (fig. S6). This suggests that the diagenetic process that added MgO and SO_3 to the Murray fm. may also have been oxidizing in nature. A potential driver of saline diagenesis can be found higher up in the stratigraphy of Mount Sharp, beneath the unconformity that defines the boundary between the upper and lower part of the Mount Sharp stratigraphy. There, hundreds of meters of stratified, sulfate mineral–bearing rocks are present, having spectral signatures consistent with the presence of the Mg sulfate mineral kieserite (*8*, *9*). It is possible that these sediments, located hundreds of meters above the base of the Murray fm., were deposited during an evaporitic phase in the evolution of the lake in Gale crater. As the fluids in this lake were driven to an increasingly saline state, they would also have become much denser and could have seeped back through the underlying stratigraphy

[e.g., (71–73)], imparting a Mg- and S-rich character to the rocks they flowed through.

The influence of rapid sedimentation on redox

Contrasting the sedimentologic character of the Sheepbed and Murray mudstones allows the influence of sedimentation rate on redox to be assessed. In particular, the Murray mudstones exhibit well developed lamination (fig. S4E), whereas the Sheepbed mudstones are massive, with only a few thin, continuous lenses of possible siltstone present (11). In terrestrial mudstones, massive bedding often reflects rapid sedimentation, which can take place when deposition occurs in close proximity to the sediment source (74). Sheepbed mudstone is directly in contact with fluvial sandstones of the Gillespie member (11), consistent with the possibility of a proximal sediment source. The Sheepbed member is also characterized by numerous early concretions, mineral-filled subaqueous shrinkage cracks, and possible fenestrae, all formed during early diagenesis (11, 20, 21); the generation of these features might also have acted to disrupt primary bedding fabrics in the Sheepbed member before lithification. The Sheepbed mudstones contain sulfide minerals of probable detrital origin and magnetite of probable authigenic origin, consistent with anoxia during deposition (18, 47–49). On the basis of these textural and mineralogical observations, we infer that the Sheepbed mudstones were isolated from the influence of atmospheric oxidants as a result of rapid deposition in a near-shore environment, in which sedimentation rates exceeded oxidation rates. As a result, detrital redox-sensitive grains were preserved, and anoxic conditions were promoted in the sediment column during Sheepbed deposition. Given the cold climate conditions implied by low-CIA values in the Sheepbed, it is plausible that sluggish redox kinetics in the cold water that characterized the lake at this time also contributed to the preservation and precipitation of reduced iron- and sulfur-bearing mineral phases (75). This mechanism of preserving and promoting anoxic conditions during deposition of the shallow-water Sheepbed member is distinct from that of the deeper water Murray MS facies, where redox stratification of the water column is implicated.

Hesperian climate and habitability

On the basis of the model we have developed (Fig. 6), we can infer a paleoenvironmental evolution from the mudstone stratigraphy in Gale crater: (i) At the base of the section, in the Sheepbed member, mudstones were deposited under cold climate conditions. Near-shore deposition, proximal to fluvial networks supplying water and clastic detritus to the lake, resulted in rapid fallout of fine-grained sediment from suspension and promoted the development of nonlaminated (massive) mudstone texture. The rapid deposition of Sheepbed sediment also acted to isolate it from atmospheric oxidants. Neutral to alkaline pH and anoxic conditions promoted the formation of authigenic phyllosilicate and magnetite. (ii) The stratigraphically higher Murray fm. was deposited under comparatively warmer and wetter climate conditions. Prograding wedges of sediment, fed by fluvial runoff, thinned with increasing transport distance, resulting in the development of finer lamination toward the center of the lake basin and segregation of detrital minerals on the basis of density and grain size. The mineralogy and geochemistry of the Murray fm. are consistent with a neutral-alkaline–pH, redox-stratified lake, in which oxidized Fe minerals and phyllosilicates were formed in the shallow portion of the lake, and mixed-valence Fe minerals and silica were formed in deeper portions. (iii) Diagenetic mineralization, possibly driven by downward migrating brines developed during a later, evaporative stage of the lake's evolution, imparted a sulfur-rich character to the Murray fm. and likely played a role in emplacing Ca sulfate–rich veins observed throughout the section.

This record from the mudstones of Gale crater challenges and confirms our current understanding of martian climate evolution. The ~100 m of stratigraphy described here indicate a climate with sufficient warmth and humidity to sustain long-lived lakes in Gale crater (10). How Mars' climate system could have achieved the conditions we interpret at Gale crater in the early Hesperian is a matter of current debate (76). In addition, comparison of the Sheepbed member to the stratigraphically higher Murray fm. indicates an evolution from a colder to a warmer climate state, with only a small component of the observed stratigraphy expressing geochemical properties consistent with a cold climate. Perhaps the climate variations apparent in the record of primary lacustrine environments in Gale crater were influenced by short-term variations, driven by impacts, volcanism, or the obliquity cycle (77, 78). The recognition of a saline diagenetic overprint on the Murray fm. is broadly consistent with the long-held idea that Mars' climate was driven from an early, wetter state to a later, more arid condition by atmospheric-loss processes (77, 79). Finally, organic carbon compounds (80, 81), nitrogen (82), phosphate minerals, and Fe and S minerals in a variety of redox states (table S1) are present in the sedimentary rocks of Gale crater. Our analysis of those rocks indicates that gradients in lake-water oxidation state were present in the primary lacustrine environment. Taken together, these results provide compelling evidence that the physical, chemical, and energetic conditions necessary to establish a habitable environment were present on Mars between 3.8 and 3.1 Ga.

Methods

We used element-oxide abundance data obtained by the APXS on board the Curiosity rover for samples analyzed between sols 129 and 487 for the Sheepbed member and sols 696 to 1091 and 1157 to 1279 for the Murray fm. All data used in this paper are available on the Planetary Data System (PDS) Geoscience Node (83) and are reproduced in data file S1 with their reported analytical uncertainties. A complete description of the instrument, and the methods used for calibration and quantification of APXS data, can be found in Gellert *et al.* (23), Campbell *et al.* (84), and the PDS (83). A brief description, modified after information publicly available on the PDS (83), is provided here: The APXS is a contact instrument that uses curium-244 sources to induce particle-induced x-ray emission (PIXE) and x-ray fluorescence (XRF). The x-ray spectra collected from soil and rock targets were used to determine the abundance of major, minor, and trace elements from sodium to bromine. Low–atomic mass (Z)–element x-rays stem from the topmost 5 μm of the sample; higher Z elements like Fe are detected from the upper ~50 μm. The APXS is mounted on a turret at the end of the Curiosity rover's arm and is deployed on selected targets along the rover traverse to determine their elemental composition. The sampled area is about 1.7 cm in diameter when the instrument is in contact with the sample, and APXS spectra represent the average composition over the sampled area.

Mineral abundances measured by the CheMin XRD instrument for the Sheepbed member samples John Klein and Cumberland, and Murray fm. samples Confidence Hills, Mojave, Telegraph Peak, and Buckskin, are derived from the following data sources: the PDS Geosciences Node (85), Morris *et al.* (31), and Rampe *et al.* (41). The measurements are reproduced in table S1 with their reported analytical uncertainties. A complete description of the CheMin instrument and the methods used for calibration and quantification of the CheMin data can be found in Blake *et al.* (22) and the PDS (85). A brief description, modified after information publicly available on the PDS (85) is provided here: The CheMin instrument is located within the body of the Curiosity rover and consists of a funnel for receiving powdered samples, 27 reusable sample cells, an x-ray source, and a cooled charge-coupled device detector. Data from the CheMin instrument are used to determine and quantify the mineralogy of powdered samples delivered by the rover's arm-mounted sample-acquisition system. Mineral identification uses various diffraction data libraries (e.g., the International Centre for Diffraction Data, Powder Diffraction File database), and pattern processing and phase quantification use a combination of several available software packages (e.g., Jade, TOPAS, FULLPAT). These approaches produce accurate identification and detection for virtually all crystalline phases at abundances greater than ~1 wt %, whereas x-ray amorphous materials have higher detection limits, with poorer accuracy in quantification.

REFERENCES AND NOTES

1. H. W. Nesbitt, G. M. Young, Early Proterozoic climates and plate motions inferred from major element chemistry of lutites. *Nature* **299**, 715–717 (1982). doi: 10.1038/299715a0
2. S. R. Taylor, S. M. McLennan, *The Continental Crust: Its Composition and Evolution*. A. Hallam, Ed. (Blackwell Scientific Publications, Oxford, 1985).
3. C. Klein, Some Precambrian banded iron-formations (BIFs) from around the world: Their age, geologic setting, mineralogy, metamorphism, geochemistry, and origin. *Am. Mineral.* **90**, 1473–1499 (2005). doi: 10.2138/am.2005.1871
4. C. Fedo, H. W. Nesbitt, G. Young, Unraveling the effects of potassium metasomatism in sedimentary rocks and paleosols, with implications for paleoweathering conditions and

provenance. *Geology* **23**, 921–924 (1995). doi: 10.1130/0091-7613(1995)023<0921:UTEOPM>2.3.CO;2
5. W. W. Fischer, A. H. Knoll, An iron shuttle for deepwater silica in Late Archean and early Paleoproterozoic iron formation. *Geol. Soc. Am. Bull.* **121**, 222–235 (2009).
6. R. Anderson, J. I. Bell, Geologic mapping and characterization of Gale Crater and implications for its potential as a Mars Science Laboratory landing site. *Mars* **5**, 76–128 (2010).
7. J. P. Grotzinger *et al*., Mars Science Laboratory Mission and science investigation. *Space Sci. Rev.* **170**, 5–56 (2012). doi: 10.1007/s11214-012-9892-2
8. R. E. Milliken, J. P. Grotzinger, B. J. Thomson, Paleoclimate of Mars as captured by the stratigraphic record in Gale Crater. *Geophys. Res. Lett.* **37**, L04201 (2010). doi: 10.1029/2009GL041870
9. B. J. Thomson *et al*., Constraints on the origin and evolution of the layered mound in Gale Crater, Mars using Mars Reconnaissance Orbiter data. *Icarus* **214**, 413–432 (2011). doi: 10.1016/j.icarus.2011.05.002
10. J. P. Grotzinger *et al*., Deposition, exhumation, and paleoclimate of an ancient lake deposit, Gale crater, Mars. *Science* **350**, aac7575 (2015). doi: 10.1126/science.aac7575; pmid: 26450214
11. J. P. Grotzinger *et al*., A habitable fluvio-lacustrine environment at Yellowknife Bay, Gale crater, Mars. *Science* **343**, 1242777 (2014). doi: 10.1126/science.1242777; pmid: 24324272
12. L. Le Deit *et al*., Sequence of infilling events in Gale Crater, Mars: Results from morphology, stratigraphy, and mineralogy. *J. Geophys. Res.* **118**, 2439–2473 (2013). doi: 10.1002/2012JE004322
13. M. C. Palucis *et al*., The origin and evolution of the Peace Vallis fan system that drains to the Curiosity landing area, Gale Crater, Mars. *J. Geophys. Res.* **119**, 705–728 (2014). doi: 10.1002/2013JE004583
14. J. A. Grant, S. A. Wilson, N. Mangold, F. Calef III, J. P. Grotzinger, The timing of alluvial activity in Gale crater, Mars. *Geophys. Res. Lett.* **41**, 1142–1148 (2014). doi: 10.1002/2013GL058909
15. T. Szabó, G. Domokos, J. P. Grotzinger, D. J. Jerolmack, Reconstructing the transport history of pebbles on Mars. *Nat. Commun.* **6**, 8366 (2015). doi: 10.1038/ncomms9366; pmid: 26460507
16. R. M. E. Williams *et al*., Martian fluvial conglomerates at Gale crater. *Science* **340**, 1068–1072 (2013). doi: 10.1126/science.1237317; pmid: 23723230
17. M. Nachon *et al*., Calcium sulfate veins characterized by ChemCam/Curiosity at Gale crater, Mars. *J. Geophys. Res.* **119**, 1991–2016 (2014). doi: 10.1002/2013JE004588
18. D. T. Vaniman *et al*., Mineralogy of a mudstone at Yellowknife Bay, Gale crater, Mars. *Science* **343**, 1243480 (2014). doi: 10.1126/science.1243480; pmid: 24324271
19. R. J. Léveillé *et al*., Chemistry of fracture-filling raised ridges in Yellowknife Bay, Gale Crater: Window into past aqueous activity and habitability on Mars. *J. Geophys. Res.* **119**, 2398–2415 (2014). doi: 10.1002/2014JE004620
20. K. L. Siebach *et al*., Subaqueous shrinkage cracks in the Sheepbed mudstone: Implications for early fluid diagenesis, Gale crater, Mars. *J. Geophys. Res.* **119**, 1597–1613 (2014). doi: 10.1002/2014JE004623
21. K. M. Stack *et al*., Diagenetic origin of nodules in the Sheepbed member, Yellowknife Bay formation, Gale crater, Mars. *J. Geophys. Res.* **119**, 1637–1664 (2014). doi: 10.1002/2014JE004617
22. D. Blake *et al*., Characterization and calibration of the CheMin mineralogical instrument on Mars Science Laboratory. *Space Sci. Rev.* **170**, 341–399 (2012). doi: 10.1007/s11214-012-9905-1
23. R. Gellert *et al*., The Alpha Particle X-Ray Spectrometer (APXS): Results from Gusev Crater and calibration report. *J. Geophys. Res.* **111**, E02S05 (2006). doi: 10.1029/2005JE002555
24. H. Bahlburg, N. Dobrzinski, in *Geological Record of Neoproterozoic Glaciations*, E. Arnaud, G. P. Halverson, G. Shields-Zhou, Eds. (Geological Society of London, 2011), vol. 36, pp. 81–92.
25. H. W. Nesbitt, in *Geochemistry of Sediments and Sedimentary Rocks: Evolutionary Considerations to Mineral Deposit-Forming Environments*, D. Lentz, Ed. (Geological Association of Canada, St. John's, 2002), vol. GEOText 4, pp. 39–51.
26. S. R. Taylor, S. M. McLennan, *Planetary Crusts: Their Composition, Origin and Evolution* (Cambridge Univ. Press, 2009).
27. S. M. McLennan *et al*., Elemental geochemistry of sedimentary rocks at Yellowknife Bay, Gale crater, Mars. *Science* **343**, 1244734 (2014). doi: 10.1126/science.1244734; pmid: 24324274
28. H. W. Nesbitt, G. M. Young, Prediction of some weathering trends of plutonic and volcanic rocks based on thermodynamic and kinetic considerations. *Geochim. Cosmochim. Acta* **48**, 1523–1534 (1984). doi: 10.1016/0016-7037(84)90408-3
29. S. M. McLennan, Sedimentary silica on Mars. *Geology* **31**, 315–318 (2003). doi: 10.1130/0091-7613(2003)031<0315:SSOM>2.0.CO;2
30. H. W. Nesbitt, R. E. Wilson, Recent chemical weathering of basalts. *Am. J. Sci.* **292**, 740–777 (1992). doi: 10.2475/ajs.292.10.740
31. R. V. Morris *et al*., Silicic volcanism on Mars evidenced by tridymite in high-SiO_2 sedimentary rock at Gale crater. *Proc. Natl. Acad. Sci. U.S.A.* **113**, 7071–7076 (2016). doi: 10.1073/pnas.1607098113; pmid: 27298370
32. N. Mangold *et al*., Composition of conglomerates analyzed by the Curiosity rover: Implications for Gale Crater crust and sediment sources. *J. Geophys. Res.* **121**, 353–387 (2016). doi: 10.1002/2015JE004977
33. K. L. Siebach *et al*., Sorting out compositional trends in sedimentary rocks of the Bradbury group (Aeolis Palus), Gale crater, Mars. *J. Geophys. Res.* **122**, 295–328 (2017). doi: 10.1002/2016JE005195
34. A. H. Treiman *et al*., Mineralogy, provenance, and diagenesis of a potassic basaltic sandstone on Mars: CheMin X-ray diffraction of the Windjana sample (Kimberley area, Gale Crater). *J. Geophys. Res. Planets* **121**, 75–106 (2016). doi: 10.1002/2015JE004932; pmid: 27134806
35. V. Sautter *et al*., *In situ* evidence for continental crust on early Mars. *Nat. Geosci.* **8**, 605–609 (2015). doi: 10.1038/ngeo2474
36. R. W. Le Maitre, The chemical variability of some common igneous rocks. *J. Petrol.* **17**, 589–598 (1976). doi: 10.1093/petrology/17.4.589
37. J. W. Tonkin, L. S. Balistrieri, J. W. Murray, Modeling sorption of divalent metal cations on hydrous manganese oxide using the diffuse double layer model. *Appl. Geochem.* **19**, 29–53 (2004). doi: 10.1016/S0883-2927(03)00115-X
38. N. L. Lanza *et al*., Oxidation of manganese in an ancient aquifer, Kimberley formation, Gale crater, Mars. *Geophys. Res. Lett.* **43**, 7398–7407 (2016). doi: 10.1002/2016GL069109
39. J. A. Berger *et al*., A global Mars dust composition refined by the Alpha-Particle X-ray Spectrometer in Gale Crater. *Geophys. Res. Lett.* **43**, 67–75 (2016). doi: 10.1002/2015GL066675
40. S. J. VanBommel *et al*., Deconvolution of distinct lithology chemistry through oversampling with the Mars Science Laboratory Alpha Particle X-Ray Spectrometer. *XRay Spectrom.* **45**, 155–161 (2016). doi: 10.1002/xrs.2681
41. E. B. Rampe *et al*., Mineralogy of an ancient lacustrine mudstone succession from the Murray formation, Gale crater, Mars. *Earth Planet. Sci. Lett.* 10.1016/j.epsl.2017.04.021 (2017). doi: 10.1016/j.epsl.2017.04.021
42. A. H. Treiman *et al*., Ferrian saponite from the Santa Monica Mountains (California, USA, Earth): Characterization as an analog for clay minerals on Mars with application to Yellowknife Bay in Gale Crater. *Am. Mineral.* **99**, 2234–2250 (2014). doi: 10.2138/am-2014-4763
43. E. Dehouck, S. M. McLennan, P. Y. Meslin, A. Cousin, Constraints on abundance, composition, and nature of X-ray amorphous components of soils and rocks at Gale crater, Mars. *J. Geophys. Res.* **119**, 2640–2657 (2014). doi: 10.1002/2014JE004716
44. H. Blatt, Provenance studies and mudrocks. *J. Sediment. Petrol.* **55**, 69–75 (1985).
45. D. B. Shaw, C. E. Weaver, The mineralogical composition of shales. *J. Sediment. Res.* **35**, 213–222 (1965).
46. J. Veizer, S. Jansen, Basement and sedimentary recycling and continental evolution. *J. Geol.* **87**, 341–370 (1979). doi: 10.1086/628425
47. T. F. Bristow *et al*., The origin and implications of clay minerals from Yellowknife Bay, Gale crater, Mars. *Am. Mineral.* **100**, 824–836 (2015). doi: 10.2138/am-2015-5077CCBYNCND
48. G. Schikorr, On the reactions between iron, its hydroxides and water. *Z. Elektrochem.* **35**, 65–70 (1929).
49. G. N. Schrauzer, T. D. Guth, Hydrogen evolving systems. 1. The formation of molecular hydrogen from aqueous suspensions of iron(II) hydroxide and reactions with reducible substrates, including molecular nitrogen. *J. Am. Chem. Soc.* **98**, 3508–3513 (1976). doi: 10.1021/ja00428a019
50. A. Stefánsson, S. Amórsson, A. E. Sveinbjörnsdóttir, Redox reactions and potentials in natural waters at disequilibrium. *Chem. Geol.* **221**, 289–311 (2005). doi: 10.1016/j.chemgeo.2005.06.003
51. B. L. Ehlmann, J. Buz, Mineralogy and fluvial history of the watersheds of Gale, Knobel, and Sharp craters: A regional context for the Mars Science Laboratory Curiosity's exploration. *Geophys. Res. Lett.* **42**, 264–273 (2015). doi: 10.1002/2014GL062553
52. C. N. Alpers, J. L. Jambor, D. K. Nordstrom, Eds., *Sulfate Minerals: Crystallography, Geochemistry, and Environmental Significance* (Mineralogical Society of America and The Geochemical Society, Washington, DC, 2000), vol. 40, p. 606.
53. R. G. Burns, D. S. Fisher, Rates of oxidative weathering on the surface of Mars. *J. Geophys. Res.* **98**, 3365–3372 (1993). doi: 10.1029/92JE02055
54. L. J. McHenry, V. Chevrier, C. Schroder, Jarosite in a Pleistocene East African saline-alkaline paleolacustrine deposit: Implications for Mars aqueous geochemistry. *J. Geophys. Res.* **116**, E04002 (2011). doi: 10.1029/2010JE003680
55. D. T. Vaniman, S. J. Chipera, D. L. Bish, Pedogenesis of siliceous calcretes at Yucca Mountain, Nevada. *Geoderma* **63**, 1–17 (1994). doi: 10.1016/0016-7061(94)90106-6
56. P. M. Dove, in *Chemical Weathering Rates of Silicate Minerals*, A. F. White, S. L. Brantley, Eds. (Mineralogical Society of America, Chantilly, VA, 1995), vol. 31, pp. 235–290.
57. W. Stumm, B. Sulzberger, The cycling iron in natural environments: Considerations based on laboratory studies of heterogeneous redox processes. *Geochim. Cosmochim. Acta* **56**, 3233–3257 (1992). doi: 10.1016/0016-7037(92)90301-X
58. P. F. Hoffman, A. J. Kaufman, G. P. Halverson, D. P. Schrag, A neoproterozoic snowball earth. *Science* **281**, 1342–1346 (1998). doi: 10.1126/science.281.5381.1342; pmid: 9721097
59. G. P. Halverson *et al*., Fe isotope and trace element geochemistry of the Neoproterozoic syn-glacial Rapitan iron formation. *Earth Planet. Sci. Lett.* **309**, 100–112 (2011). doi: 10.1016/j.epsl.2011.06.021
60. N. J. Beukes, C. Klein, in *The Proterozoic Biosphere: A Multidisciplinary Study*, J. W. Schopf, C. Klein, Eds. (Cambridge Univ. Press, 1990), pp. 147–151.
61. G. M. Cox *et al*., Neoproterozoic iron formation: An evaluation of its temporal, environmental and tectonic significance. *Chem. Geol.* **362**, 232–249 (2013). doi: 10.1016/j.chemgeo.2013.08.002
62. G. M. Marion, R. E. Farren, Mineral solubilities in the Na-K-Mg-Ca-Cl-SO_4-H_2O system: A re-evaluation of the sulfate chemistry in the Spencer-Moller-Weare model. *Geochim. Cosmochim. Acta* **63**, 1305–1318 (1999). doi: 10.1016/S0016-7037(99)00102-7
63. A. M. Baldridge *et al*., Contemporaneous deposition of phyllosilicates and sulfates: Using Australian acidic saline lake deposits to describe geochemical variability on Mars. *Geophys. Res. Lett.* **36**, L19201 (2009). doi: 10.1029/2009GL040069
64. K. C. Benison, B. B. Bowen, Acid saline lake systems give clues about past environments and the search for life on Mars. *Icarus* **183**, 225–229 (2006). doi: 10.1016/j.icarus.2006.02.018
65. J. M. McArthur, J. V. Turner, W. B. Lyons, A. O. Osborn, M. F. Thirlwall, Hydrochemistry on the Yilgarn Block, western Australia: Ferrolysis and mineralization in acidic brines. *Geochim. Cosmochim. Acta* **55**, 1273–1288 (1991). doi: 10.1016/0016-7037(91)90306-P
66. K. M. Bohacs, A. R. Carroll, J. E. Neal, P. J. Mankiewicz, in *Lake Basins Through Space and Time*, E. H. Gierlowski, K. R. Kelts, Eds. (American Association of Petroleum Geologists, Tulsa, OK, 2000), vol. 46, pp. 3–34.
67. R. V. Demicco, L. A. Hardie, Eds., *Sedimentary Structures and Early Diagenetic Features of Shallow Marine Carbonate Deposits* (Society for Sedimentary Geology, Tulsa, OK, 1994), vol. 1.
68. J. Grotzinger *et al*., Sedimentary textures formed by aqueous processes, Erebus crater, Meridiani Planum, Mars. *Geology* **34**, 1085–1088 (2006). doi: 10.1130/G22985A.1
69. B. C. Schreiber, M. El Tabakh, Deposition and early alteration of evaporites. *Sedimentology* **47**, 215–238 (2000). doi: 10.1046/j.1365-3091.2000.00002.x
70. B. W. Logan, *The Macleod Evaporite Basin, Western Australia: Holocene Environments, Sediments, and Geological Evolution, Memoir No. 44* (American Association of Petroleum Geologists, Tulsa, OK, 1987).
71. J. E. Adams, M. L. Rhodes, Dolomitization by seepage refluxion. *Am. Assoc. Pet. Geol. Bull.* **44**, 1912–1920 (1960).
72. A. B. Al-Helal, F. F. Whitaker, Y. T. Xiao, Reactive transport modeling of brine reflux: Dolomitization, anhydrite precipitation, and porosity evolution. *J. Sediment. Res.* **82**, 196–215 (2012). doi: 10.2110/jsr.2012.14
73. G. D. Jones, P. L. Smart, F. F. Whitaker, B. J. Rostron, H. G. Machel, Numerical modeling of reflux dolomitization in the Grosmont platform complex (Upper Devonian), Western

Canada sedimentary basin. *Am. Assoc. Pet. Geol. Bull.* **87**, 1273–1298 (2003).
74. P. E. Potter, J. B. Maynard, W. A. Pryor, *Sedimentology of Shale: Study Guide and Reference Source* (Springer, 1980).
75. W. Stumm, G. F. Lee, Oxygenation of ferrous iron. *Ind. Eng. Chem.* **53**, 143–146 (1961). doi: 10.1021/ie50614a030
76. R. D. Wordsworth, L. Kerber, R. T. Pierrehumbert, F. Forget, J. W. Head, Comparison of "warm and wet" and "cold and icy" scenarios for early Mars in a 3-D climate model. *J. Geophys. Res.* **120**, 1201–1219 (2015). doi: 10.1002/2015JE004787
77. M. H. Carr, J. W. Head III, Geologic history of Mars. *Earth Planet. Sci. Lett.* **294**, 185–203 (2010). doi: 10.1016/j.epsl.2009.06.042
78. J. Laskar *et al*., Long term evolution and chaotic diffusion of the insolation quantities of Mars. *Icarus* **170**, 343–364 (2004). doi: 10.1016/j.icarus.2004.04.005
79. J. P. Bibring *et al*., Global mineralogical and aqueous mars history derived from OMEGA/Mars Express data. *Science* **312**, 400–404 (2006). doi: 10.1126/science.1122659; pmid: 16627738
80. C. Freissinet *et al*., Organic molecules in the Sheepbed Mudstone, Gale Crater, Mars. *J. Geophys. Res. Planets* **120**, 495–514 (2015). doi: 10.1002/2014JE004737; pmid: 26690960
81. K. E. Miller *et al*., Potential precursor compounds for chlorohydrocarbons detected in Gale Crater, Mars, by the SAM instrument suite on the Curiosity Rover. *J. Geophys. Res.* **121**, 296–308 (2016). doi: 10.1002/2015JE004939
82. J. C. Stern *et al*., Evidence for indigenous nitrogen in sedimentary and aeolian deposits from the Curiosity rover investigations at Gale crater, Mars. *Proc. Natl. Acad. Sci. U.S.A.* **112**, 4245–4250 (2015). doi: 10.1073/pnas.1420932112; pmid: 25831544
83. R. Gellert, Mars Science Laboratory Alpha Particle X-Ray Spectrometer RDR data V1.0, MSL-M-APXS-4/5-RDR-V1.0 (NASA Planetary Data System, 2013).
84. J. L. Campbell *et al*., Calibration of the Mars Science Laboratory Alpha Particle X-ray Spectrometer. *Space Sci. Rev.* **170**, 319–340 (2012). doi: 10.1007/s11214-012-9873-5
85. D. Vaniman, Mars Science Laboratory Chemistry and Mineralogy RDR data V1.0, MSL-M-CHEMIN-5-RDR-V1.0 (NASA Planetary Data System, 2012).
86. D. E. Smith *et al*., Mars Orbiter Laser Altimeter: Experiment summary after the first year of global mapping of Mars. *J. Geophys. Res.* **106**, 23689–23722 (2001). doi: 10.1029/2000JE001364

ACKNOWLEDGMENTS

We are indebted to the MSL project's engineering and management teams for their efforts in making the mission effective and enhancing science operations. We are also grateful to those MSL team members who participated in tactical and strategic operations, without whom the data presented here could not have been collected. J.A.H. acknowledges support from a subcontract from the NASA Jet Propulsion Laboratory, California Institute of Technology. J.P.G. acknowledges the support of the NASA Astrobiology Institute. A.G.F. was supported by the Project "icyMARS," European Research Council Starting Grant no. 307496. J.F. acknowledges the support from the Villum Foundation. R.G. and M.E.S. acknowledge support from the Canadian Space Agency, which is responsible for funding the APXS instrument and its operations. Data presented in this paper are archived in the Planetary Data System at http://pds-geosciences.wustl.edu/missions/msl/index.htm. Three anonymous reviewers are acknowledged for their contributions.

SUPPLEMENTARY MATERIALS

www.sciencemag.org/content/356/6341/eaah6849/suppl/DC1
Supplementary Text
Figs. S1 to S6
Table S1
Data File S1
References (*87*–*99*)

31 July 2016; accepted 19 April 2017
10.1126/science.aah6849

Redox stratification of an ancient lake in Gale crater, Mars

J. A. Hurowitz, J. P. Grotzinger, W. W. Fischer, S. M. McLennan, R. E. Milliken, N. Stein, A. R. Vasavada, D. F. Blake, E. Dehouck, J. L. Eigenbrode, A. G. Fairén, J. Frydenvang, R. Gellert, J. A. Grant, S. Gupta, K. E. Herkenhoff, D. W. Ming, E. B. Rampe, M. E. Schmidt, K. L. Siebach, K. Stack-Morgan, D. Y. Sumner and R. C. Wiens

Science **356** (6341), eaah6849.
DOI: 10.1126/science.aah6849

The depths of an ancient lake on Mars

Gale crater on Mars was once a lake fed by rivers and groundwater. Hurowitz *et al*. analyzed 3.5 years of data from the Curiosity rover's exploration of Gale crater to determine the chemical conditions in the ancient lake. Close to the surface, there were plenty of oxidizing agents and rocks formed from large, dense grains, whereas the deeper layers had more reducing agents and were formed from finer material. This redox stratification led to very different environments in different layers, which provides evidence for Martian climate change. The results will aid our understanding of where and when Mars was once habitable.

Science, this issue p. eaah6849